Glacial Inception on Baffin Island: The Interaction of Ice Flow and Meteorology

Leah Birch[1], Timothy Cronin[2], and Eli Tziperman[1]

[1]School of Engineering and applied Sciences and Department of Earth and Planetary Sciences, Harvard University, Cambridge, MA, USA
[2]Department of Earth, Atmosphere and Planetary Sciences, MIT, Cambridge, MA, USA

Correspondence to: Leah Birch (lbirch@seas.harvard.edu)

Abstract. Over the past 0.8 million years, 100 kyr ice ages have dominated Earth's climate with geological evidence suggesting the last glacial inception began in the mountains of Baffin Island. Currently, state-of-the-art global climate models (GCMs) have difficulty simulating glacial inception, possibly due in part to their coarse horizontal resolution and the neglect of ice flow dynamics in some models. We attempt to address the initial inception problem on Baffin Island by asynchronously coupling

5 the Weather Research and Forecast model (WRF), configured as a high resolution inner domain over Baffin and an outer domain incorporating much of North America, to an ice flow model using the shallow ice approximation. The mass balance is calculated from WRF simulations, and used to drive the ice model, which updates the ice extent and elevation, that then serve as inputs to the next WRF run. We drive the regional WRF configuration using atmospheric boundary conditions from 1986 that correspond to a relatively cold summer, and with 115 kya insolation. Initially, ice accumulates on mountain glaciers,

10 driving downslope ice flow which expands the size of the ice caps. However, continued iterations of the atmosphere and ice models reveal a stagnation of the ice sheet on Baffin Island, driven by melting due to warmer temperatures at the margins of the ice caps. This warming is caused by changes in the larger-scale circulation that are forced by elevation changes due to the ice growth. A stabilizing feedback between ice elevation and atmospheric circulation thus prevents full inception from occurring.

1 Introduction

15 For the past million years, Earth's climate has repeatedly fallen into ice ages with a periodicity of $\sim 100,000$ years (Petit et al., 1999). The start of an ice age is called glacial inception and is a largely unresolved problem in climate science (Otieno and Bromwich, 2009). The leading hypothesis for the cause of glacial inception is that orbital variations (Milankovitch, 1941) cause cooler summers leading to less melting, which can be further amplified by positive feedbacks associated with greater height and extent of mountain glaciers (Lee and North, 1995; Oerlemans, 2002; Abe-Ouchi et al., 2007). These positive feedbacks then

20 lead to runaway growth ice growth, creating ice sheets that span continents. Additional feedbacks between ice elevation and atmospheric circulation might modify both the accumulation and ablation patterns on an incipient ice sheet (Roe and Lindzen, 2001a). In this study, we seek to understand these critical ice-climate feedbacks associated with glacial inception using a regional climate model asynchronously coupled to a simple ice sheet model. Our regional model is centered over Baffin Island – the likely location of the last glacial inception (Ives, 1962; Ives et al., 1975; Clark et al., 1993).

Glacial inception of the Laurentide ice sheet is thought to have progressed fairly rapidly in eastern Canada (Clark et al., 1993), with the associated drop in sea level estimated to be as large as 50 m in 10kyrs (Waelbroeck et al., 2002; Ganopolski
5   et al., 2010). The Laurentide ice sheet has been identified as the primary initial cause of the drop in sea level (Kleman et al., 2013) and some simulations have shown rapid inception within a few thousand years (Andrews and Mahaffy, 1976; Marshall and Clarke, 1999). However, this rapid growth required the precipitation to be tripled or the climate cooled by 2 degrees every thousand years, without any explicit explanation. A more modest sea level drop 10-20 m in 10 kyrs has also been posited (Lambeck and Chappell, 2001; Creveling et al., 2017), which indicates a slower ice sheet growth rate and possibly ice growth
10 relegated to Arctic Canadian Islands (Kleman et al., 2002).

Global climate models (GCMs) have been used to simulate glacial inception, but often fail because snow fails to accumulate in unglaciated areas, nor do glaciers spread into unglaciated areas. One reason GCMs have difficulty simulating the glacial inception is their coarse horizontal resolution, which lowers the topographic features dramatically (Wang and Mysak, 2002; Vettoretti and Peltier, 2003). Snow then does not accumulate because the region is too warm due to artificially low elevations
15 (Rind et al., 1989). Though topography is important (Oerlemans, 2002; Marshall and Clarke, 1999), other aspects of the climate system may also be misrepresented or neglected in GCMs, like ocean feedbacks (Khodri et al., 2001), dust (Calov et al., 2005; Farrell and Abbot, 2012), sea ice (Gildor and Tziperman, 2001; Li et al., 2005), vegetation (Wang et al., 2005; Goñi et al., 2005), and meteorology (Bromwich et al., 2002; Jackson and Broccoli, 2003; Birch et al., 2017). Increasing the model resolution has lead to moderate improvements in the simulation of glacial inception (Jochum et al., 2012; Vavrus et al., 2011), through the
20 occurrence of areas of net snow accumulation, which can progressively expand as the climate cools.

Cool summer temperatures are critical for inception, and while Milankovitch forcing explains some summer cooling, the large scale circulation is an important driver of heat and moisture fluxes to inception areas. In the current climatology, large scale cyclonic circulation over Baffin Bay is associated with cool summers (Bromwich et al., 2002; Gardner and Sharp, 2007), which may be all that is necessary for inception. However, Jackson and Broccoli (2003) and Khodri et al. (2001) also noted increased
25 storms and poleward moisture fluxes during inception. Otieno and Bromwich (2009) showed that in addition to favorable circulation and temperature, snow could accumulate in new areas only after artificial large-scale cooling was prescribed. The question remains: how does this cooling occur? One possible answer is the interaction of ice sheets and the atmosphere.

As the ice sheet grows, it influences the atmosphere due to albedo and surface elevation changes. The large scale circulation can also be diverted by the changing topography. Anti-cyclones have been noted to occur over mountains (Smith, 1979), but
30 ultimately, the effects of mountains on the regional climate and large-scale circulation depends on the mean overlying flow and mountain size (Chen and Lin, 2005; Cook and Held, 1988). Looking at ice growth in the context of glacial inception, Roe and Lindzen (2001a) argued using a simple model that slight changes in topography can influence the stationary waves, significantly changing the circulation and leading to colder temperatures. The topography and geographic location may be critical to the glacial inception process (Jackson, 2000; Abe-Ouchi et al., 2013).

35 To capture the interaction of ice and the atmosphere, climate models of intermediate complexity have been combined with ice sheet models. This type of coupled ice-climate model allows thousands of years of ice growth due to changes in insolation and CO_2 to be simulated. Often, however, these models glaciate Alaska and Western Canada very rapidly (Kageyama et al., 2004;

Bonelli et al., 2009; Ganopolski et al., 2010), which is not consistent with the geological record showing inception occurred first in eastern Canada (Clark et al., 1993). Ice sheet models and GCM studies (Dong and Valdes, 1995; Meissner et al., 2003)

5   have a similar problem of not agreeing with the geological record. Combining GCMs and ice sheet modeling may allow for progress in understanding ice-atmosphere interactions (Herrington and Poulsen, 2011; Gregory et al., 2012; Löfverström et al., 2014), but the smoothed topography and other biases in these coarse resolution climate models often need to be artificially corrected to obtain an accurate regional climate. Furthermore, mountain ice caps of the Canadian Arctic Archipelago in the present climate are too small to be modeled by most GCMs.

10   The interaction of the ice and the atmosphere is critical to inception. Birch et al. (2017) used a high-resolution cloud-permitting regional climate model and found that ice would accumulate on the mountain glaciers of Baffin Island. The 4 km resolution of that study allowed us to capture both the ablation and accumulation zones of mountain glaciers. By integrating the mass balance from the top of the ice cap down slope, Birch et al. (2017) implicitly represented the effects of ice flow. As a result, the Penny Ice Cap was deduced to grow outside of its present day bounds due to decreased insolation and a sequence of

15   cold summers and wet winters. Consistent with previous GCM studies, no snow accumulated in unglaciated areas. Thus, the purpose of the current paper is to explicitly include ice flow from the growing mountain glaciers, allowing us to investigate the feedbacks between a growing ice sheet and the atmosphere at higher spatial resolution than can be simulated with GCMs. For this purpose, we use a simple ice model based on the shallow ice approximation, asynchronously coupled with the Weather Research and Forecasting model (WRF, Skamarock et al., 2008). We find that the change to ice sheet topography induces

20   an anticyclonic atmospheric response over Baffin Island. This anticyclone causes a flow of warm air over Baffin Island and Hudson Bay area, increasing ablation, stagnating further ice sheet growth, and thus indicating a negative feedback on inception at the regional scale. This is reminiscent to the findings of Herrington and Poulsen (2011) and Gregory et al. (2012) who noted the continued growth of the ice sheet is slowed by changes in large scale circulation that arise from atmosphere-topography interactions. While the studies of Herrington and Poulsen (2011) and Gregory et al. (2012) found the negative feedback slowed

25   ice growth mostly when the ice sheet was fairly developed, of a continental-scale, the negative feedback analyzed here occurs upon inception, as soon as the ice caps over the Baffin Island begins to grow. Previous studies (Herrington and Poulsen, 2011; Gregory et al., 2012) could not resolve this feedback with their coarse resolution GCMs, while our coupled ice sheet - regional atmospheric model enables us to examine it.

The atmospheric and ice models used for the asynchronous coupling experiment are presented in Section 2. We present

30   the results in Section 3, beginning with ice thickness and mass balances of our atmosphere-ice iterations. We then investigate the regional and large-scale impacts of expanding ice cover and increasing ice elevation. Sensitivity simulations exploring the importance of topography and insolation are also presented. Finally, the sensitivity of ice flow to ice viscosity and mass balance are examined. We conclude with a discussion in Section 4, including the limitations of this study and its implications.

2 Methods

Our goal in this study is to better understand the interaction between changing ice cover and the regional climate of Baffin Island and the large-scale circulation over North America. We therefore use a nested configuration of the Weather Research and Forecasting Model (WRF Skamarock et al., 2008) with the outer domain covering all of North America with a 100 km resolution and the inner domain covering Baffin Island with a 20 km resolution, encompassing both the Penny and Barnes Ice

5 Caps. To better understand the growth of these mountain glaciers during inception, we must simulate ice flow in the inner 20km resolution domain, but WRF does not contain an ice flow model, which means the ice expansion must be calculated offline. Based off of Oerlemans (1981), we developed a simple ice flow model that reduces the 3D Stokes flow to two dimensions using the shallow ice approximation. The basal sliding velocity is assumed to be 0. This approximation results in a nonlinear diffusion equation that represents ice flow by evolving ice thickness H in time based on horizontal gradients of surface elevation

10 H*, along with surface mass balance G:

$$\frac{\partial H}{\partial t} = \nabla \cdot D \nabla H^* + G \qquad (1)$$

In Equation 1, the yearly surface mass balance G is calculated from WRF simulations and assumes that the density of ice is 900 kg m^{-3}. The surface elevation H^* and ice thickness H are linked by $H^* = B + H$, where B is the basal topography. The nonlinear shear-thinning of ice flow is represented by a diffusivity, D, which depends on both the ice thickness and surface

15 elevation gradients:

$$D = AH^{m+2}\left[\left(\frac{\partial H^*}{\partial x}\right)^2 + \left(\frac{\partial H^*}{\partial y}\right)^2\right]^{(m-1)/2} \qquad (2)$$

The parameter m for all model simulations is set to 3, which is a typical value for realistic ice simulations Cuffey and Paterson (2010). The coefficient A in Equation 2 is the creep parameter that influences the viscosity of the ice is based on the temperature of the ice, i.e. the colder ice flows more slowly, while warmer ice more quickly. We use a creep parameter

20 $A = 3.5 \times 10^{-25}$ Pa^{-3}s^{-1} from Cuffey and Paterson (2010), which was evaluated at a temperature of -10°C. More details on this choice of creep parameter can be found in Appendix A, which also contains the details of the numerical scheme used to integrate this ice model in time.

The ice model requires the specification of surface elevation (H^*), ice thickness (H), and mass balance (G) as inputs. The ice thickness (H) is adapted from the present day ice cover on Baffin Island from NASA Operation IceBridge Mission (Kurtz

25 and Farrell, 2011), while H^* and G are taken from our WRF simulations. The grid size and time step are also user specified and chosen to be 20 km (same as WRF inner domain) and 1-year, respectively. With these atmospheric and ice models, we perform iterations, running WRF, using the mass balance calculated by WRF to force the ice model, updating the ice thickness and extent calculated by the ice model, and then running WRF again with the newly calculated ice cover as an input. This amounts to an asynchronous coupling of the two models, where a WRF run followed by the ice model is considered an iteration.

30   WRF (Skamarock et al., 2008), version 3.7, is a compressible, non-hydrostatic model, which has been shown to provide a reasonable simulation of Arctic regions (Cassano et al., 2011; Kilpeläinen et al., 2011). Reanalysis data from the European Centre for Medium-Range Weather Forecasts (ECMWF, Dee et al., 2011) are used for setting the meteorological boundary and initial conditions, including sea surface temperatures and sea ice extent. Cassano et al. (2011) also noted that the Interim re-analysis (ERA-Interim) is a suitable choice of boundary conditions for WRF, leading to minimal bias in the Arctic, specifically

5   in temperature.

We use the WRF Single Moment 6 Class microphysics scheme, which allows for ice, snow and graupel processes (Hong and Lim, 2006). NOAH-MP (Niu et al., 2011) is used for the land surface model. It includes 4 layers of snow and allows for refreezing, which is an important process on the Penny Ice Cap according to historical trends (Zdanowicz et al., 2012). NOAH-MP caps the snow water content at $2000 \, \mathrm{kg \, m^{-2}}$ by default, but we remove this limit. The radiation scheme is the

10   Rapid Radiative Transfer Model for GCM applications (RRTMG, Iacono et al., 2008), which has been found to have minimal bias in WRF (Cassano et al., 2011). CO_2 is set to 290 ppm for a glacial inception scenario (Petit et al., 1999; Vettoretti and Peltier, 2004). The boundary layer is simulated with the Mellor-Yamada-Janic scheme (MYJ, Janjic, 1994). We do not nudge to observations in any way other than prescribed lateral boundary conditions at the edges of our outer domain. Note that these physics are the same as those used in our previous paper (Birch et al., 2017), except now we use the Grell convective scheme

15   (Grell and Dévényi, 2002), which has been shown to give good results in present day (Hines et al., 2011) and LGM (Bromwich et al., 2005) Arctic climates.

With this WRF configuration we find a reasonable reproduction of the ECMWF atmospheric state when we simulate present-day climate. Furthermore, precipitation on the coast of Baffin Island matches observations at that point of about 300 mm per year (Zdanowicz et al., 2012). Greenland is initialized with present day ice cover and elevation based on studies finding little

20   influence of Greenland on the build up of the Laurentide ice sheet (Kubatzki et al., 2006).

The incoming solar radiation is set to values consistent with 115 kya; the process of modifying the insolation in WRF based on the orbital parameters is detailed in Appendix B. We use realistic present day land type from the WRF database as initial conditions for the ice extent. Over these land grid points classified as ice, a snow water equivalent (SWE) of $5000 \, \mathrm{kg \, m^{-2}}$ is prescribed — sufficient for maintaining snow cover for the duration of our runs and allowing us to capture a representative

25   yearly mass balance for the chosen climatology.

2.1 Asynchronous Coupling Procedure

We begin our WRF-ice flow coupled model experiment with the WRF control simulation, which uses meteorology from October 1985 to October 1986. The circulation during this year brought the coldest and wettest extremes to Baffin Island (Bromwich et al., 2002) and causes the present day ice cover to expand when combined with 115 kya insolation (Birch et al.,

30   2017). WRF is run for 5 years, but we only analyze the last 4 years for an average climatology. Accumulation occurs over areas initialized with ice cover at high elevations, and net mass balance is positive, allowing ice growth (Fig. 1a). The control simulation agrees with our previous 4 km simulation of the Penny Ice Cap (Birch et al., 2017): cold meteorology causes the positive mass balance needed for the ice cap to expand. This mass balance is then adapted for use in the ice model.
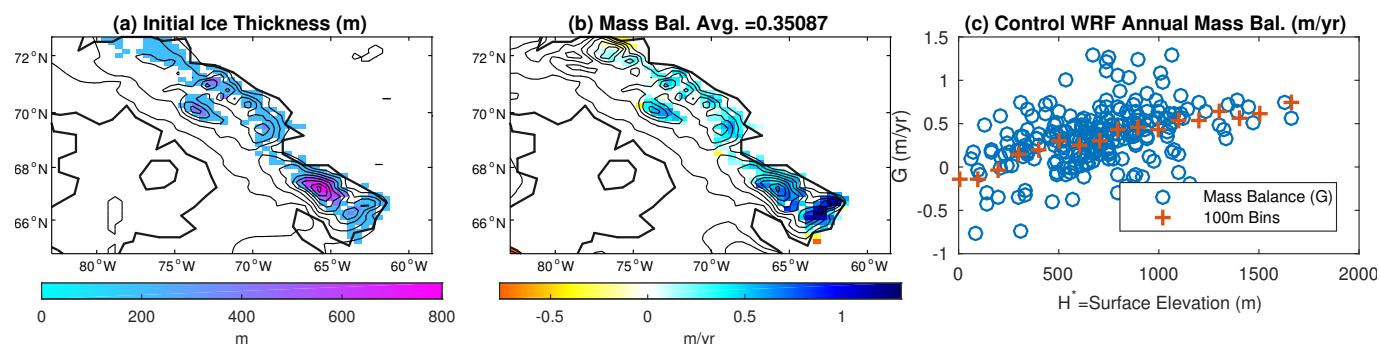
Figure 1. Ice thickness and Mass Balance for Ice Sheet Initialization: (a) Ice thickness was adapted from data collected by the NASA Operation IceBridge Mission (Kurtz and Farrell, 2011) with extent set by land use type in WRF. (b) Annual Mass Balance from WRF Control Run.(c) Binned Regression Visualization

For the first iteration of the ice model, initial ice thickness is adapted from present day ice cover from the NASA Operation IceBridge Mission (Fig. 1a). We use the surface elevation from the 20km resolution control WRF domain. The mass balance needed to force the ice model is calculated from the WRF simulation. Figure 1b depicts the mass balance results from the control WRF simulation with cold meteorology, 115 kya insolation, and present day ice cover. The mass balance over the ice caps is generally positive, except on the edges of the ice cap where there is net ablation. Over the rest of the domain, WRF

5 cannot calculate a meaningful annual mass balance because all snowfall received melts off during the summer. We characterize the mass balance as a function of elevation ($G(H^*)$), which allows the mass balance at each grid point to be updated as the surface elevation and ice thickness change every time step. This characterization involves sorting the domain by surface elevation and forming bins every 100 m. The average the mass balance in each bin is depicted by the purple crosses in Fig. 1c. Note the plateau in the mass balance at high elevations, which is expected from the elevation desert effect.

10 For our asynchronous coupling experiment, the ice model is run for 500 years, which was judged appropriate by Herrington and Poulsen (2011). After 500 years, the ice model has calculated a new ice extent and surface elevation (Fig. 2a) with which to force WRF. We import the surface elevation directly into the 20 km resolution WRF domain and use the ice extent to update the land type, i.e., the expansion of the ice cap. Much like our control simulation, over areas classified as ice, we prescribe a snow depth of 5000 kg m^{-2}. The surface elevation and land type of the 100 km resolution parent domain are adjusted through

15 interpolation of the 20km resolution surface elevation and land type. Soil temperatures from the previous WRF run are used to initialize the next WRF iteration. In our simulations, soil temperatures take a year to equilibrate, leading us to agree with de Noblet et al. (1996) that present day soil temperatures are too warm. Again using 115 kya insolation and cold meteorology, WRF is run for 5 years to characterize the mass balance on this new ice cap. This new run is the start of the next iteration. Thus, each iteration begins with a WRF run and ends after the 500-year ice model integration.

3   Results

20

In the context of glacial inception, expanding ice cover interacts with the atmosphere, causing changes to both the regional climate of Baffin Island and the large-scale circulation. We first examine the progression of the WRF-ice model iterations, looking at the expansion of ice cover and the resultant changes in mass balance. Then, in Section 3.1, the changes in mass balance are explained by exploring changes in temperature, ablation, precipitation, and cloud cover. In section 3.2, we take

5   a closer look at the large-scale circulation. Additional sensitivity simulations with the ice sheet model further clarify climate factors that could lead to Baffin Island glaciation in Section 3.5.

The progression of WRF-ice model iterations (5 years of WRF and 500 years of the ice model) is laid out in Figure 2. The ice thickness calculated by the ice model and then used in WRF is depicted in the left column, and the resulting annual mass balance from WRF in the right column. Also included in the right column is the spatial average of mass balance on the ice cap

10   (defined as all grid cells with ice land cover type). Starting with the top left, we show the ice thickness resulting from running the ice model for 500 years using the control WRF mass balance. This new ice thickness, ice extent, and surface elevation computed by the ice model are used as inputs to the next WRF simulations. Then WRF is run for 5 years with the mass balance presented in the right column. After the second iteration of WRF, we bin the mass balance by elevation, and force the ice model with the new updated mass balance. A new ice cover is computed (left row, second column) and used as an input in

15   WRF. Subsequent iterations pictured follow the same procedure.

The second iteration has the greatest ice extent, which is due to the large positive control mass balance. In the third iteration, the ice retreats from its margins, though there is still growth in the highest parts of the domain. Additional iterations show that the ice cap coalesces and increases in thickness to nearly 2000 m, but expands slowly into new areas. After 5 kyrs, the ice accumulation on Baffin Island would only lower global sea level by 0.6 m. Although the average mass balance does generally

20   increase with time, the rest of our analysis focuses on why the ice does not expand quickly.

The binned mass balance used in the ice model is plotted in Figure 3 with annual mass balance on the y-axis and surface elevation on the x-axis. The control WRF run is the "+" blue line with the highest mass balance, particularly at the lowest and highest elevations. In subsequent WRF runs, the mass balance up to 1000 m becomes more negative at low elevations, which we find surprising. One might expect the equilibrium line to shift downslope as a result of regional cooling from the initial

25   expansion of the ice cover, leading to a more positive mass balance. However, plotting the binned mass balance for all iterations shows a general trend of increasingly more negative mass balances at low elevations, with the equilibrium line altitude shifting upwards by several hundred meters over the course of ten iterations. As a result, the ice caps coalesce and thicken at high elevations, but stagnate and fail to expand horizontally. The mass balance at highest elevations from all iterations also illustrate desertification, or the mass balance becoming less positive over time as the ice cap increases in height and its top surface

30   flattens.

Lateral expansion is slow because the lower terrain on Baffin Island is not strongly sloped. Thus, ice must build up to a substantial height before the spread of ice outweighs ablation at the ice edge. For example, with flat basal topography, calculations based on equations 1 and 2 suggest that a 0.5 m/yr of ice thickness increase due to ice flow in a grid cell with
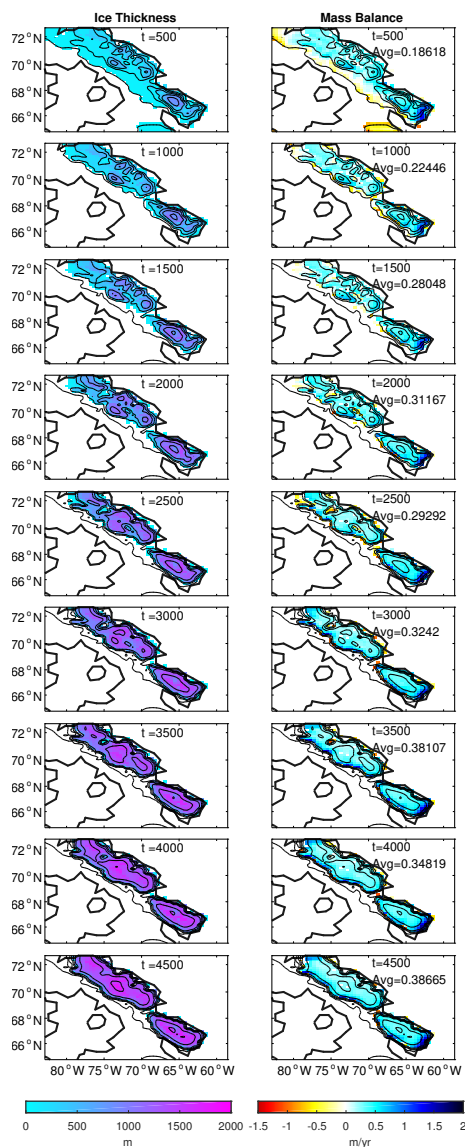
Figure 2. Ice growth due to WRF-ice model iterations. Left column is the ice thickness from the ice sheet model. Right column is the mass balance from WRF. The average mass balance over ice-covered areas for each iteration is included in the right column.
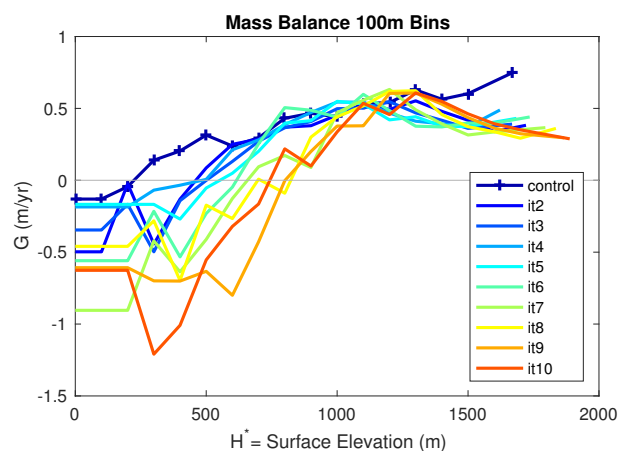
Figure 3. Characterizing annual mass balance vs. surface elevation. The domain is sorted into 100 m bins and within each bin the mass balance is averaged. Elevations falling within the range of the bin have the associated mass balance.

no ice requires an adjacent grid cell ice thickness around 500 m. This approximate ice thickness on the margins occurs in our simulations as depicted in Figure 2.

3.1 Mechanisms of Changes in Mass Balance

A closer examination of temperature, melting, and precipitation can help us how the ice cap growth causes the changes to mass balance in the WRF simulations. We begin with the 2 m temperature on Baffin Island during the summer (June, July,

5 August) when melting occurs. The differences in the temperature between the control run and subsequent iterations are pictured in Figure 4. In the control simulation, we note that most of the ice-covered land remains below freezing during the summer (blue). At the edge of the ice cap, temperatures generally remain near zero (white), and the low elevation tundra is above freezing (red). The largest expansion of ice cover occurs in the second iteration as noted above, which dramatically cools much of the region mostly due to the presence of snow and the albedo change. Also note that the upper part of the ice cap also

10 cools, likely due to increasing elevation, since 500 years of ice growth increased the surface elevation by 200 m. In the third iteration, the ice has retreated somewhat, which makes the low elevations warmer than in the second iteration. The integrated mass balance becomes more positive as seen in Figure 2. As iterations of WRF and the ice model continue, we find that the area covered in ice cools, but the low-elevation tundra area surrounding the ice cap warms. The lapse rate effect due to increasing surface elevation progressively cools the ice cap, and below we explore why the low-elevation tundra warms in successive

15 iterations.

The mass balance is made up of ablation and precipitation. When precipitation is larger than ablation, the ice cap grows. We are interested in how both variables change over the iterations of the coupled WRF-ice sheet models. We start by examining the melting over the summer, and how it relates to the temperature discussed above. Figure 5a depicts the yearly melt in control simulation. In general, the high elevation parts of the region experience no melting during the summer, due to their sub-freezing
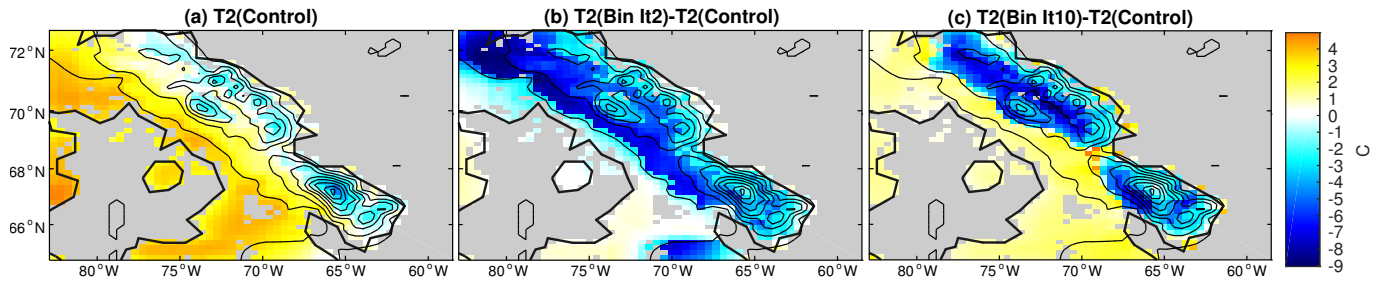
Figure 4. The Summer 2m Temperature in select asynchronous coupling iterations: (a) The temperature in control WRF. Differences in temperature between control and (b) second and (c) last iterations.
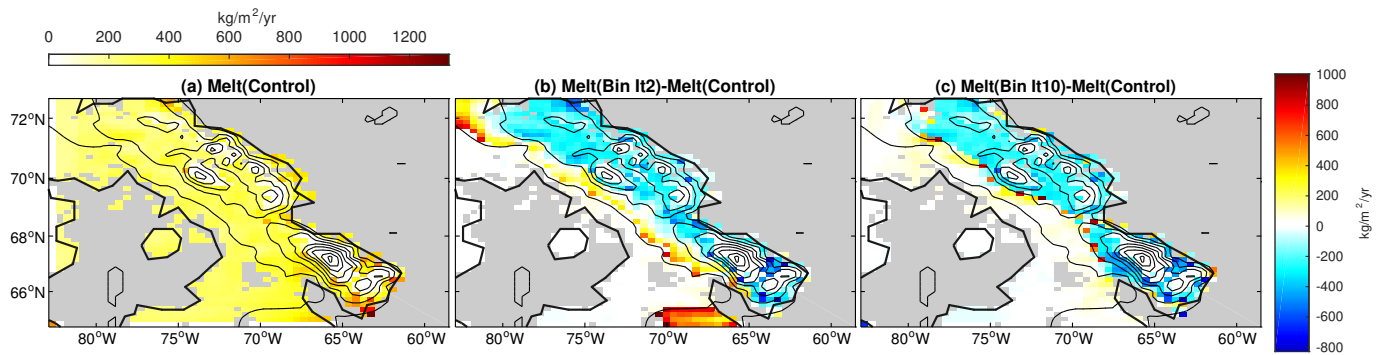

Figure 5. Melting in WRF in select iterations: (a) melting in the control WRF run. Differences in melting between control and (b) second and (c) last iterations.

20   temperatures. As the ice cover expands, the highest values of melting are located near the edges of the ice cap. As expected, melting decreases as the surface elevation increases.
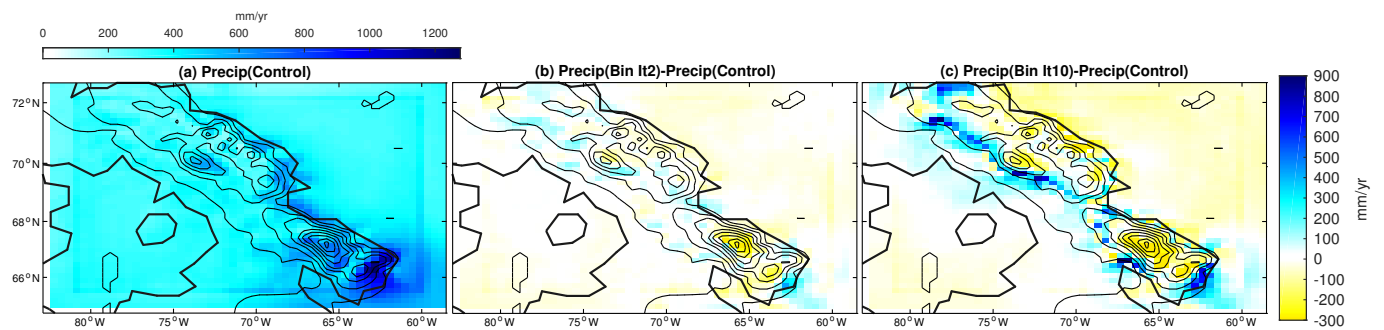

Figure 6. Annual precipitation in WRF in select iterations: (a) The precipitation in the control WRF run. Precipitation differences between control and (b) second and (c) last iterations.
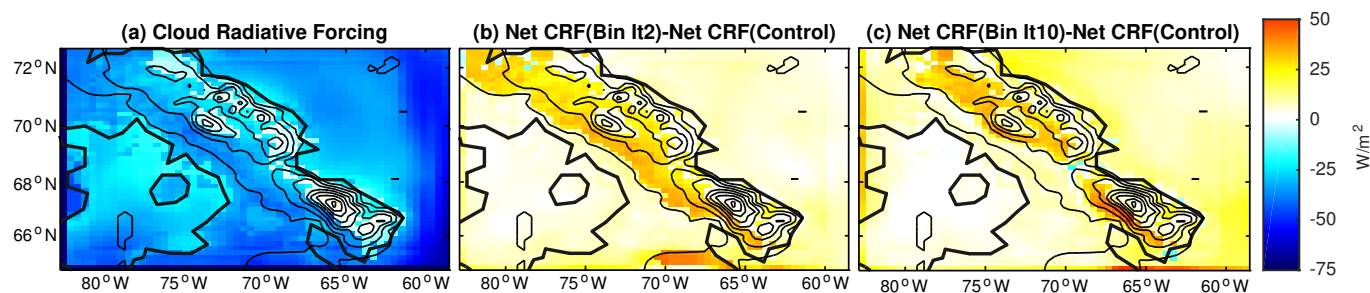
Climate
of the Past
Discussions

Figure 7. The Summer Cloud Radiative Forcing (CRF) in select iterations: (a) The CRF in the control WRF run. Differences in CRF in (b) second and (c) last iterations.

Next, we look at the precipitation component of the mass balance. In this region, precipitation increases with elevation due to the orography (Figure 6). For glacial inception, continued snowfall is critical in addition to low ablation. Figures 6b and c depict the differences in precipitation between the control simulation and ice model iterations. We see an elevation desert effect that reduces precipitation by 200 mm year^{-1}, or $\sim 20\%$ of the annual precipitation. The highest elevations receive less precipitation as the iterations go on. However, at the edges of the ice cap, precipitation increases, because the change in

5   elevation and surface slope triggers orographic precipitation there. It is interesting that precipitation increases with ice growth on the Barnes region of the ice cap, which may be a necessary condition for glacial inception to occur. The accumulation increases on the western side of Baffin Island, which is also the windward side and as noted by Roe and Lindzen (2001b), a characteristic of the inception process. This general increase in precipitation near the margins agrees with the maps of the mass balance (Fig. 2) indicating the greatest mass balances do not occur on the peaks of the island, but at about 1200 m elevation.

10   Finally, we are interested in the role that clouds may play in glacial inception. Jochum et al. (2012) and Birch et al. (2017) found clouds to be negative feedback during glacial inception. When insolation is changed from present day to that appropriate for the time of glacial inception at 115 kya, Jochum et al. (2012) noted that less low clouds form during glacial inception, while Birch et al. (2017) found that cloud properties change such that relative to present day, less shortwave is blocked from the surface. Our objective here is to examine this feedback during the integration of our asynchronously coupled model. In

15   Figure 7, the net CRF in the control simulation is negative during the summer because the clouds block shortwave radiation from reaching the surface. However, as the ice cover expands, the clouds block less shortwave radiation, illustrated by the positive net shortwave CRF difference between later iterations and the control run: the control simulation net CRF is more negative in all parts of the domain. The albedo of increasing snow cover accounts for less negative CRF over newly glaciated areas, but the change to the shortwave CRF in the rest of the domain is due to changes in cloud cover and properties.

20   **3.2   Interaction of Baffin Island Inception and Large-Scale Atmospheric Circulation**

We find the significant warming over Baffin Island to be surprising, as one might expect the expanded ice cover over the peaks of Baffin Island to lead to cooling (which would amplify the positive mass balance and lead to a larger ice sheet). We now
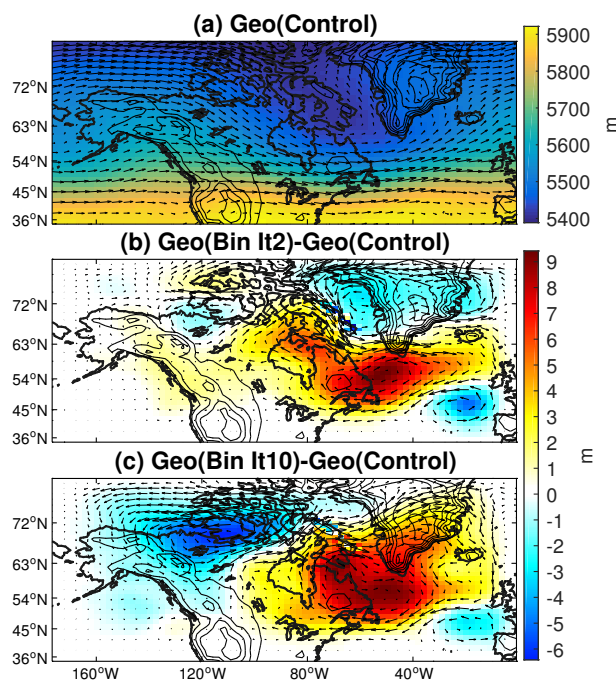
Figure 8. Changes in 500-mbar geopotential height in the Parent Domain in select iterations with wind vectors. Wind speeds are 6 m s^{-1} over Baffin Island. (a) The 500-mbar geopotential height for the control simulation with average largescale flow during the summer (b)-(c) 500-mbar geopotential hegith differences during the summer between control and iterations. Wind anomalies of 1 m s^{-1} are overlaid.
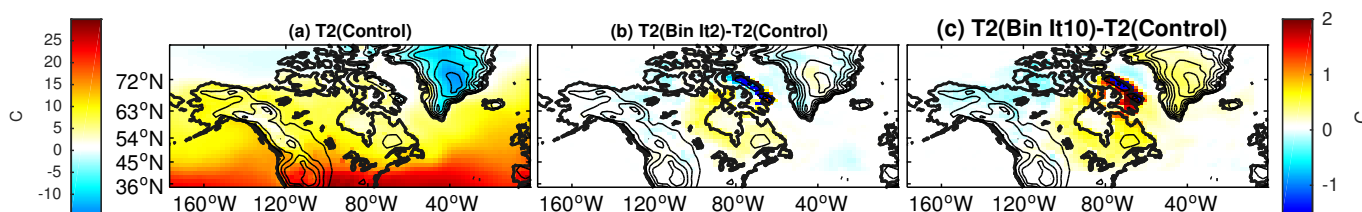

Figure 9. Summer 2m Temperature in the Parent Domain in select iterations: (a) The 2m Temperature for the control simulation (b)-(c) 2m Temperature differences during the summer between control and iterations.

analyze the warming by looking at the larger scale geopotential height field, temperature, and winds in the outer domain. First, the geopotential height and winds at 500 mbar for the control simulation during the summer are depicted in Fig. 8. The wind field over Baffin Island generally comes from the northwest with a low pressure trough covering the whole island. A weak cyclonic flow also exists over the island and Baffin Bay. Next we examine the subsequent iterations and their anomalies in the winds and geopotential height at 500 mbar in Figs. 8b-c. The pressure increases south of Baffin Island while it decreases over

5   Baffin Bay to the north, and an anomalous anticyclone forms over the Hudson Bay region. It seems that the larger ice caps on Baffin Island alter the circulation, and we will examine this hypothesis below.

The 2m temperature response in the outer domain (Figure 9) is consistent with the changes in geopotential height. The control simulation is depicted in the upper left with subsequent panels showing differences in the following iterations. On the ice caps of Baffin Island, the temperature generally grows colder because the elevation has increased, and newly glaciated areas cool due to both the presence of ice and the elevation increase. As iterations progress, the non-glaciated points of the island warm, which is also seen in the inner domain. Additionally, warming occurs outside of Baffin Island in the Hudson Bay region.

5   These areas of warming, coinciding with geopotential height anomalies, appear to be caused by the circulation response, with warm southerly advection by the anomalous anticyclone.

This warming appears to be a negative feedback on ice sheet growth, and it explains the mass balances becoming more negative at low elevations on Baffin Island through subsequent iterations (Fig. 3). With a region so close to freezing during the summer even a degree warming can prevent perennial snow from occurring during the critical inception period.

10 As a caveat, we note that with the topography in the coarser outer domain being generally lower than the 20km resolution domain, the temperatures on Baffin Island are much warmer than is likely realistic. For instance we do not see any summer temperatures significantly below freezing as found in the inner domain with more realistic topography.

3.3   The of Impact Baffin Island Ice Elevation on Large-Scale Circulation

Next, we diagnose the roles of ice and topography on circulation changes, by setting up sensitivity simulations based on the
15 second iteration, which has changes in ice extent and surface elevation (Fig.2). For our "No H" scenario, we keep the surface elevation the same as the control simulation, but use the same ice extent as in the second iteration. For an "H Only" scenario, we remove all ice, changing the land type classification to tundra. We then set the surface elevation to the ice height in the second iteration. These two additional simulations were run for 5 years with cold meteorology and 115 kya insolation and the analysis focuses on the last 4 years.

20 In Figure 10, we examine the temperature of the outer domain for 4 experiments. Again, the control simulation summer temperature and difference from the second iteration (having both ice and elevation changes) are shown, but we also include the "No H" and "H Only", in c and d respectively. With "No H", a significant regional cooling occurs, encompassing both Baffin Island and the Hudson Bay region, which is the pattern we had anticipated to cause rapid ice growth. However, with "H Only", warming on both Baffin Island and around Hudson Bay occurs. Thus, the cause of the negative feedback due to large
25 scale anticyclonic circulation and warming in our simulations is the change in topography. An interesting aspect of these last two simulations ("No H" and "H Only") is that if we sum the difference between their response and the control simulation, the result is very close to the difference between iteration two and the control run, as seen in Fig. 11. This indicates that the responses to the ice topography and ice land type (albedo and other surface properties) are linear.

3.4   Glacial Inception with Changing Orbital Parameters

30 The WRF-ice model iterations performed previously used the minimum insolation from 115kya, which is useful for diagnosing the relationship between the ice cover and atmosphere. However, that is obviously not realistic. Integrated insolation increased after its minimum at 115 kya, impacting temperature and glacial mass balance. We use the procedure detailed in the Appendix
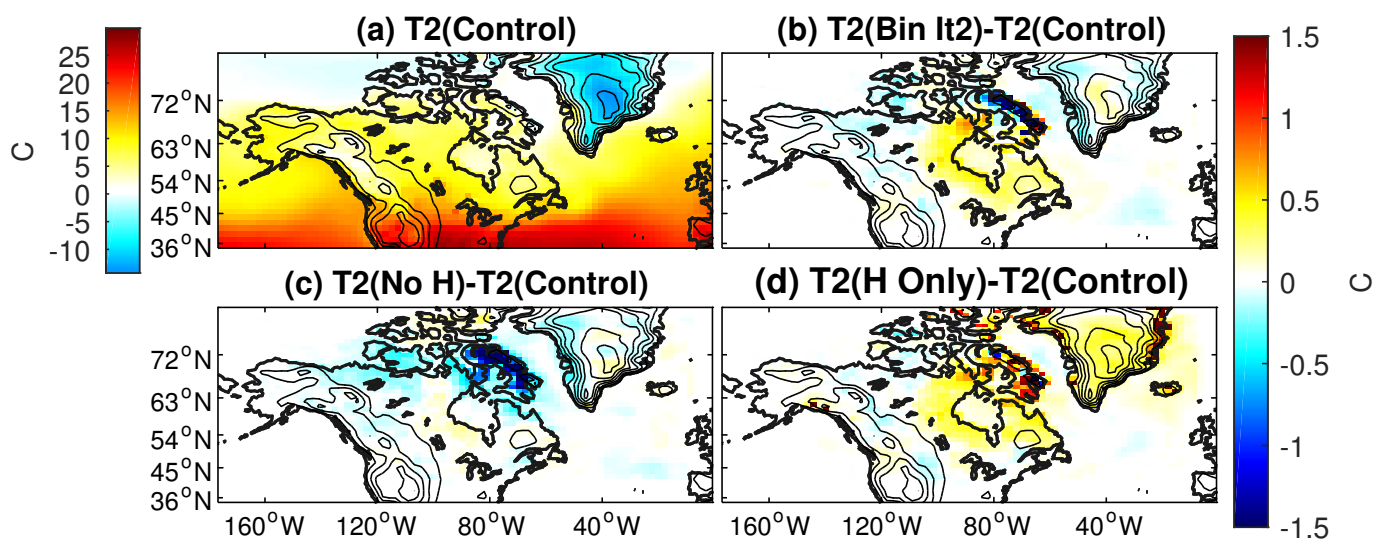
Figure 10. Changes in 2m Summer Temperature in the Parent Domain for topography and ice sensitivity simulations. (a) The 2m Temperature for the control simulation with averaged large-scale flow during the summer (b) differences during the summer between control and second iterations. (c) differences between the control and No H. (d) differences between control and H Only.
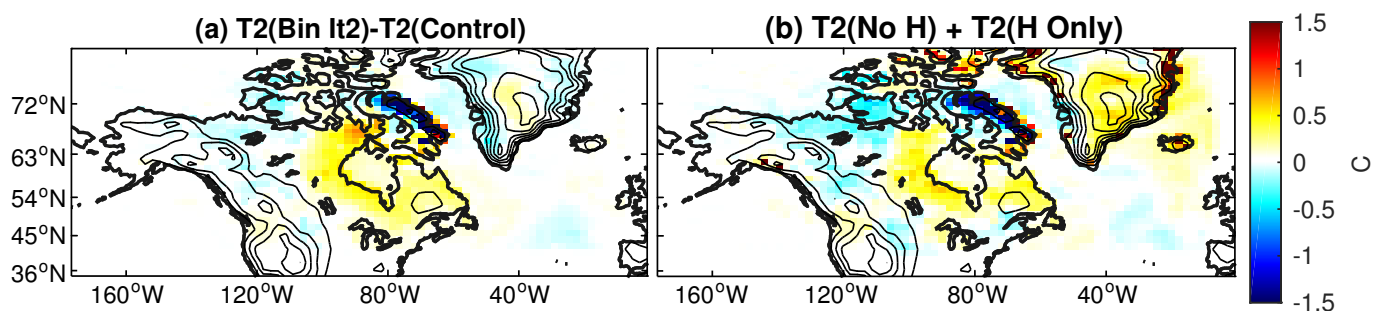

Figure 11. (a) Differences during the summer 2m temperature between control and second iterations. (b) Sum of temperature differences from "No H" and "H Only" scenarios, implying a linear response due to changes in ice cover and surface elevation
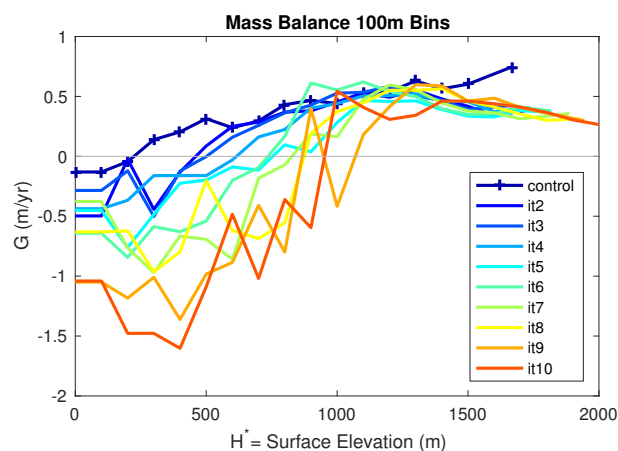
Figure 12. The Mass Balance Binned by Elevation used in simulations with realistic insolation from 115 kya to 111 kya, where the control simulation and iteration 2 uses 115 kya insolation and iteration 10 uses 111 kya.

of Birch et al. (2017) to set the insolation in WRF for 115-111 kya. After each WRF run, the ice model is integrated for 500 years using the same mass balance procedure as detailed above. This set of simulations explores the mass balance that results from a combination of ice flow and insolation changes.

Figure 12 presents the mass balances calculated from WRF and used in each iteration of the ice model. Note the control simulation and 2nd iteration plotted here are the same as presented in Figure 3 because the change in insolation occurs at 114
5 kya, which is the third iteration in Fig. 12. The elevation desert effect is again observed and the mass balances become more negative at low elevations, hindering lateral growth. Thus, these iterations progress in a similar manner as the case with constant insolation in that the lateral growth is slow though the height of the ice sheets does grow, but the high elevation plateaus can be 200 m lower than the previous set of simulations with constant 115 kya. In this set of simulations with realistic insolation the mass balances at low elevations are more negative, explaining the slower growth (Fig. 12).

10 During the summer on Baffin Island, there is again cooling from the presence of ice, but the unglaciated parts of Baffin Island warm considerably. As the summer insolation increases, the summer temperature of all of North America, not just the Hudson Bay region, increases as well. When we look at the precipitation in the domain, we observe a similar pattern to the previous set of simulations. Accumulation increases on the edges of the ice cap due to orographic precipitation. Then at the top of the ice cap, the elevation desert effect kicks in. The ice cap continually receives less precipitation than in the control simulation.
15 The increases in insolation causes continental-scale warming, and when combined with topography changes, the warming on Baffin Island can be over 5 K (Figure 13). Thus, the realistic insolation changes cause further warming during inception, which makes the occurrence of inception even more difficult to explain and simulate.
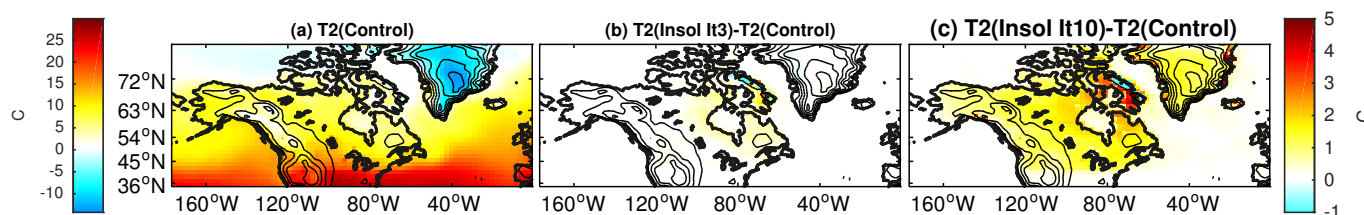
**Climate
of the Past**
Discussions

Open Access EGU

Figure 13. The surface temperature in the control and differences for successive iterations.
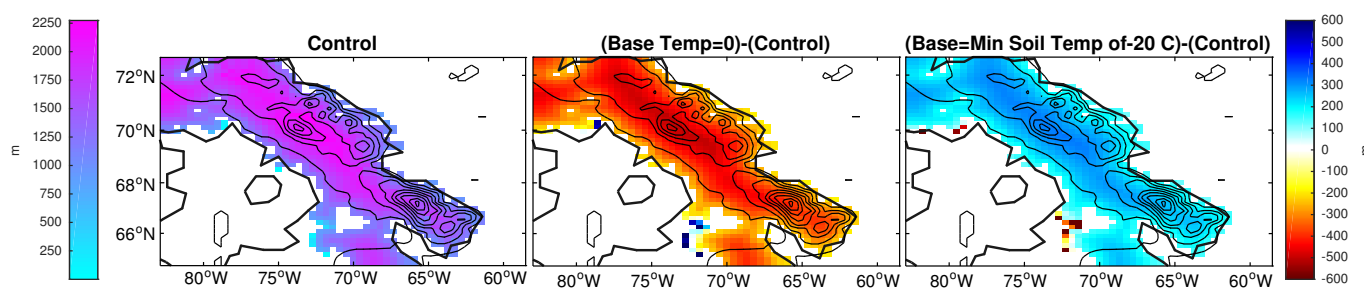

Figure 14. Sensitivity of the Ice Model to choice of constant creep parameter $A(T)$, which is related to the temperature profile within the ice as detailed by Cuffey and Paterson (2010). (a) A evaluated at $-10°$C or A($-10°$)C. (b) A($0°$C). (c) A($-15°$)C

3.5 Sensitivity Analysis of the Ice Flow Model

The combination of WRF and the ice flow model does not indicate ice sheets would grow to cover all of Baffin Island, which would likely be necessary to explain the sea-level drop found in the paleorecord. The change in ice surface elevation actually causes a negative feedback on inception by affecting the large scale circulation: temperatures around the ice increase inhibiting ice expansion. This result suggests a closer examination of the ice model and its sensitivities. In particular, we vary the creep

5   parameter A to see if rapid ice expansion is possible with different constant choices. We also explore how a successful inception - matching paleorecord estimates - could occur from our simulated mass balance function $G(H^*)$ and limiting the calving loss of ice in Hudson Bay. The ice model in these sensitivity experiments is now run for 10kyrs, unlike our previous asynchronous simulations that ran for 5 kyrs total.

First, we identify if we have simulated a mass balance sufficient for a successful inception. From Figure 3, we note that
10   the mass balance in the control simulation is the most positive at high elevations and least negative at low elevations. All subsequent WRF runs simulate a negative mass balance at low surface elevations. Using the control mass balance, the ice model is integrated over 10 kyrs. Of course, this situation is not realistic as our set of simulations show changes in mass balance due to circulation changes as the ice sheet grows. We prescribe the mass balance only on Baffin Island, which was the location of our inner domain, and this causes Baffin Island to be mostly covered by ice, corresponding to 1.75 m sea level drop
15   over 10 kyrs. Ice model simulations forced with the mass balances from iterations 2-10 do not reach the western coast of Baffin Island in 10kyrs.
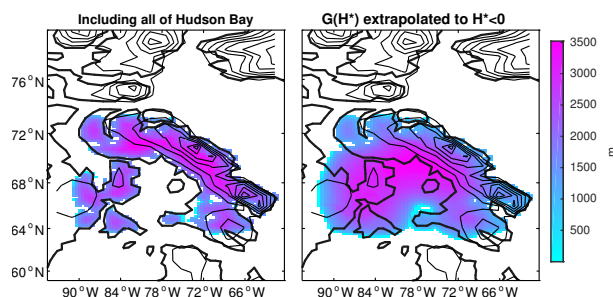
Figure 15. The result of running the ice model for 10kyrs with the maximum mass balance, found in the first WRF iteration. (a) Allowing a positive mass balance on mainland Canada, surrounding all of Hudson Bay. (b) G(H*) extrapolated to H*<0 in Hudson Bay, which allows for ice flow instead of immediate calving of ice.

As noted above, we choose the creep parameter ($A(T) = A(-10°C)$) based on Cuffey and Paterson (2010). We now test the sensitivity of the ice flow when $A(T)$ is evaluated at warmer and colder temperatures, or A(0°C) and A(-15°C) respectively. For these simulations, the mass balance used is from the control WRF simulations, and when run for 500 years, the ice model changes are minor. We confirm with WRF simulations that these slight changes in ice elevation from A(0°C) and A(-15°) do not significantly affect the mass balance in the second iteration; the ice still retreats. Thus, we want to examine how the

5   creep parameter affects ice flow on longer timescales, which is why we integrate the ice model in time for 10 kyrs. We expect that a warmer temperature and thus larger A would allow the ice to spread more easily, leading to larger ice cover.Figure 14 shows that changing the creep parameter can increase or decrease the thickness of a Baffin island ice cap by about 20%, but does not alter the ice extent much after 10 kyr. On average, $A(-10°C)$ causes the elevation to be 200 m higher than $A(0°C)$. More calving occurs with $A(0°C)$ ice reaches the coast sooner. We also examine the impact of temperatures at about $-15°C$

10 (Fig. 14c), which Marshall et al. (2002) determined to be the basal temperature of the initial ice sheet growth. As expected, the ice flows more slowly and accumulates at high elevations. These sensitivities to the creep parameter, however, are small compared to the sensitivity of ice extent and thickness to the mass balance G(H*) as inferred from successive iterations of WRF.

We also question what would happen if we apply the control mass balance to a larger area, outside of Baffin Island and

15 our chosen domain. Based on the temperature and precipitation patterns of the outer domain, the other side of Hudson Bay could have a similar mass balance, especially if the domain were resolved at a higher resolution. We do not include the Torngat Mountains on mainland Canada just to the south of Baffin Island, as this area appears to receive less precipitation and experience higher temperatures. This agrees with observations and other ice modeling simulations showing later glaciation in this area. The ice accumulation with the positive mass balance from our control WRF simulation on mainland Canada causes

20 an equivalent sea level drop of 2.8 m in 10 kyrs.

The previous simulations assume immediate calving over any ocean points, which makes sense for the kilometer deep Baffin Bay. The topography on the eastern side of Baffin Island is steep, possibly preventing ice shelves from forming. However, Hudson Bay is only about 200 m deep. We turn off immediate calving for this shallow water body, and instead prescribe a

Climate
of the Past

Discussions

negative mass balance. We extend the regression $G(H)$ linearly to the bathymetry of Hudson Bay. This allows for ice to flow slowly into a larger area surrounding Baffin Island, creating a fairly large ice sheet and corresponding to a sea level drop of 6.6 m. This last scenario gets close to more recent constraints of sea level drop from modeling simulations at around 100 kya of 10m (Creveling et al., 2017). This growth of the ice sheet corresponds a successful inception, though still on the slower side of observational constraints, suggesting that the negative feedback due to the response of the large scale circulation to expanding

5   ice cover is what prevents our asynchronously coupled model from achieving a successful inception.

4   Discussion

In this paper, we have attempted to simulate the last glacial inception beginning at 115kya with a regional high resolution configuration of WRF, coupled asynchronously with a simple ice flow model. A net positive mass balance occurs in the 1st WRF iteration simulation driven by 115 kya insolation, cold present day (1986) boundary conditions, and present day ice

10   cover, which could cover all of Baffin Island in an ice sheet after 10 kyr if that mass balance was maintained. However, updating the ice cover and surface elevation in WRF creates a negative feedback from changes in the large scale circulation: summer temperatures over Baffin Island increase due to a large-scale anticyclonic circulation. This causes the mass balance over Baffin Island to become more negative at low elevations, stagnating further ice expansion in the ice flow model.

The flow over Baffin Island driven by the 1986 boundary conditions is consistently from the northwest during the summer,

15   with weak speeds of about 6 m s^{-1} at 500 mbar. The increase in the ice surface elevation after the 1st iterations of the coupled model causes an anticyclonic response of about 1 m s^{-1} to develop to the south of Baffin Island while a cyclone develops in the north, diverting the winds and bringing in warmer air from the south. This leads to net ablation and arrests the glaciation process. This circulation response is likely dependent on the initial flow (direction and speed) and topographic height (Chen and Lin, 2005; Cook and Held, 1988). Thus, a different meteorology choice might lead to sustained accumulation. Bromwich et al.

20   (2002) identified exceptionally cold conditions on Baffin Island and their varying large scale circulation patterns. Generally, the cold summer circulation flows from the northwest or north-north-west. We examine the role of meteorology directly using boundary conditions that differ from those used in our cold meteorology simulations. For this purpose, WRF is driven using 1979 boundary conditions, which is an average year in regards to temperature and precipitation, and the flow over Baffin Island generally comes from the west. WRF simulates a negative mass balance for this year, and the ice sheet retreats to a elevations

25   above 1400 m when the ice model is forced with this mass balance for 500 years. In contrast, the ice cap from our average 1979 meteorology at a 4 km resolution was in approximate equilibrium, leaning towards slight expansion (Birch et al., 2017). Net ablation occurs in the 20 km resolution because of the lower topography. It is possible that during inception that the circulation pattern was different and allowed for both the initial ice expansion and continued cold conditions. WRF did not simulate such a pattern in this study, nor did we have a large sample of "cold" meteorological conditions in the ERA-Interim reanalysis.

30   We find significant warming on Baffin Island and the surrounding Hudson Bay region in response to the initial ice growth due to anticyclonic flow. The formation of anticyclones over expanding ice sheets has been noted to allow cold northerly winds to flow over the ice sheet, enhancing inception (Roe and Lindzen, 2001b; Liakka et al., 2012). In particular, small ice sheets

cause a wave response that enhances accumulation, while stationary waves induce less cooling as ice sheets increase in size (Liakka and Nilsson, 2010). In contrast, the anticyclone in our simulations forms south of the ice growing on Baffin Island, bringing significant warming even over these relatively small mountain glaciers. Similar to our study, Herrington and Poulsen (2011) found the Hudson Bay warmed in their coupled atmosphere-ice simulations due to anticyclonic flow. Gregory et al. (2012) also found warming on the margins from anticylones and reduced cloudiness. In both of these studies, though, the

5   warming only slowed growth; the regional cooling due to the growing ice sheet kept the ice advancing. We find the heat fluxes into the region by the developing anticyclone circulation to completely overpower any regional cooling from the snow albedo feedback, stagnating the ice sheet growth. We do observe the development of katabatic winds in response to ice sheet growth in our model, possibly contributing to the drying out of the region and decreasing cloud cover, but these winds do not cool the area outside of the glaciers sufficiently to allow for inception.

10   We do not find a positive feedback that would lead to a more positive mass balance due to the initial ice growth. However, some of our assumptions and modeling choices could be preventing such a positive feedback. For instance, our WRF simulations prescribe the SSTs and sea ice to those of 1986, but during glacial inception the SST would likely decrease and sea ice extent grow larger (Meissner et al., 2003). Allowing the SST to cool has been shown to induce cooling over land, even if the atmosphere is warm (Yoshimori et al., 2002), and Kageyama and Valdes (2000) noted that storm tracks change with colder

15   SSTs. The amount of sea ice can impact accumulation over the ice sheet (Yin and Battisti, 2001; Kubatzki et al., 2006) due to decreasing atmospheric moisture and evaporation from ocean, according to the temperature precipitation feedback (Källén et al., 1979; Ghil, 1994; Gildor and Tziperman, 2000, 2001; Li et al., 2005). Some studies argued that the cooling during inception did not cause sea ice to extend outside of Baffin Bay until 80kya (Löfverström et al., 2014), meaning the Atlantic remained ice free, which was conducive to high precipitation. Goñi et al. (2005) also argued that SSTs remained warm until

20   105 kya, when substantial ice sheets had formed. Both Khodri et al. (2001) and Wang and Mysak (2002) found that including ocean feedbacks caused increased moisture fluxes conducive to inception, while Jackson and Broccoli (2003) and Kaspar et al. (2007) noted that storm frequency increased. Including ocean feedbacks could lead to increased moisture fluxes and thus precipitation, or it could lead to cooler temperatures decreasing melting, which could be more important for inception. In either case, using present day ocean SSTs is likely inaccurate, but more work is needed to understand the impact of the ocean.

25   We also fix the CO_2 concentration to 290 ppm, although CO_2 decreased during inception. This decrease has been shown to influence the accumulation of northern hemisphere ice sheets (Ganopolski and Calov, 2011; Vettoretti and Peltier, 2004), accounting for up to 50% more ice (Bonelli et al., 2009). We also do not allow for dynamic vegetation, but on Baffin Island this should not matter. Most of these studies dealing with dynamic vegetation refer to the treeline moving southward during glacial inception (Harvey, 1989; Goñi et al., 2005), enhancing ice growth, but on Baffin Island the vegetation is mostly tundra

30   and shrubs, which are not an impediment to snow accumulation as trees would be (Otterman et al., 1984).

We choose to drive our model with 1986 boundary conditions based on the anomalous increase in precipitation and cool temperatures over Baffin Island. The large-scale flow induced by these boundary conditions in conjunction with ice growth causes the negative feedback discussed above, but it is possible that a complete reorganization of the pattern of Northern Hemisphere stationary waves could occur as part of the inception process, which we cannot capture with our regional model

35   and prescribed boundary conditions. The Laurentide ice sheet and Fennoscandian ice sheet in Europe are thought to have begun growing at the same time though the Laurentide increased in volume more rapidly (Kleman et al., 2013; Ganopolski et al., 2010). The European ice sheet may have influenced the formation of the Laurentide (Beghin et al., 2014), but such a feedback is missing in our regional model. Roe and Lindzen (2001b) noted that changes in the stationary wave pattern would affect the downstream climate, "the possiblity of a complicated set of interactions in which each of the two major Northern

5   Hemisphere ice sheet influences evolution of the other".

We limit our study to Baffin Island based on geological records of it being the nucleation of the Laurentide, but regional modeling of other Canadian mountain ranges could help identify how easily other areas glaciated, contributing to sea level drop. Growth of ice at high elevations simultaneously throughout Eastern Canada is not impossible, which could all coalesce into the Laurentide. For instance, various ice sheet models have shown ice beginning to accumulate all over Canada (Andrews

10   and Mahaffy, 1976; Marshall and Clarke, 1999). While many of these ice modes do not match geological records because they simulate the growth of ice in the West, ice growth on many of the more eastern mountain ranges could perhaps impact the large-scale circulation in a manner conducive to inception.

Though we do find net accumulation in our control simulation using a 20 km resolution, there are inherent issues that come from this resolution. The topography of Baffin Island is very rough, but is greatly smoothed by the 20 km resolution. More

15   importantly, the highest elevation peaks with 20 km resolution is ~ 400 m below the peaks found in realistic Baffin Island topography. Our simulation with average meteorology demonstrates that resolution changes can switch the mass balance from net accumulation to net ablation. For cold meteorology, the resulting mass balance is similar to what we found with a 4 km resolution (Birch et al., 2017).

To get an average mass balance to drive the ice sheet model, WRF is run for 5 years; we use the average mass balance

20   from the last 4 years. We find that the land model required a 1 year spin up time, although often a spin up time of more than a year is recommended (Yang et al., 1995; Cosgrove et al., 2003). We tested running the model for longer than 10 years, but the simulations did not deviate much from years 2-5 of our simulations. Deser et al. (2014) showed that multiple ensemble members of an atmospheric model simulation can give different results on a time scale up to 50 years, but this may not be an issue here because we are driving our regional model with boundary conditions that constrain the synoptic and planetary-scale

25   flows (Denis et al., 2002).

Using the shallow ice approximation neglects important ice dynamics, in particular it neglects lateral stresses and does not allow for the development of ice streams, which cause rapid ice flow. It has also been suggested that a finer grid size in the ice model could make for more accurate flow, as coarser resolutions have been shown to halt ice flow (Van den Berg et al., 2006). As noted above, lateral expansion only occurs when substantial ice thickness exists in an adjacent grid cell. However,

30   we find that simulations with a 4km resolution yield similar ice flow patterns to the 20 km results we present above. We are neglecting basal sliding that may develop as the ice base melts due to geothermal heat flux (Marshall and Clark, 2002). The initiating ice sheet was likely frozen at the bed (Marshall et al., 2000), which makes our choice appropriate. Finally, we are not accounting for glacial isostatic adjustment. Herrington and Poulsen (2011) found that the isostatic adjustment was not critical for glacial inception, though including the adjustment revealed a small positive feedback. Therefore, contrary to conventional

35 wisdom, these studies suggest that isostatic adjustment might actually favor glacial inception over Baffin Island, and may even
be critical to the process by reducing the strength of negative elevation-circulation feedbacks on ice growth (as in the "No H"
sensitivity test).

Though we find negative feedbacks on the growth of ice sheets due to clouds and large-scale circulation preventing inception
in our model, high resolution regional modeling still has potential to make progress on the inception problem. We have captured

5 the mass balance on critical mountainous regions in our control run, which GCMs cannot simulate accurately. When combined
with ice flow, the control mass balance causes a significant portion of Baffin Island and the surrounding area to become ice
covered. Though the equivalent sea level drop is only 6 m in 10 kyrs, the geological constraints on sea level drop from the
Laurentide are not tight. We do find this equivalent sea level drop is closing in on more recent sea level estimates (Creveling
et al., 2017). The temperature and precipitation in this scenario is not very different from present day, meaning maintaining

10 this meteorology could be all that is necessary for inception. The warming feedback of the large-scale circulation could be
mitigated by changes in the pattern of atmospheric stationary waves. Using a circumpolar regional model is the logical next
step because it can capture the mass balance of the nucleation points of both the Laurentide and Fennoscandian ice sheets, as
well as exploring the possible impact of a smaller Greenland ice sheet upon exiting the last interglacial.

Appendix A: Shallow Ice Model Set-Up

The simple ice sheet model is based off of Oerlemans (1981), where ice flow is represented by a non-linear diffusion equation and the diffusivity contains a constant term called the creep factor. This parameter determines the ice viscosity and depends on the temperature of the ice (Cuffey and Paterson, 2010), meaning it can be denoted $A(T)$ as illustrated in Equation A1:

$$A(T) = A_0 e^{-Q/RT} \tag{A1}$$

5

If $T < -10\text{C}$, then $A_0 = 3.61 \times 10^{-13}$ Pa^{-3} s^{-1} and $Q = 60 \times 10^3$ J mol^{-1}, but if $T \geq -10\text{C}$, then $A_0 = 1.734 \times 10^3$ Pa^{-3} s^{-1} and $Q = 139 \times 10^3$ J mol^{-1}.

The surface of the ice is colder than the base, meaning that throughout a real ice sheet temperature, and thus $A(T)$, vary. In fact, the basal temperature often reaches $0°$C for thick enough ice sheets. For an ice model using the shallow ice approxima-

10 tion the standard procedure is to take the vertical average of $A(T)$ (Weertman, 1957; Goodman and Pierrehumbert, 2003) in Equation A2:

$$A(T) = \frac{1}{h} A(T(z)) dz \tag{A2}$$

Since $A(T(z))$ varies by height, we need a vertical temperature profile of our ice sheet, which WRF does not provide. We

15 can calculate one using the average temperature of the ice surface from WRF and the geothermal heat flux of 55 W m^{-1} over Baffin Island, assuming a linear vertical temperature profile. Then we evaluate $A(T)$ for this temperature profile as found in Equation A and take the vertical average. Typically, this vertical average captures $A(T)$ at warmer temperatures at the base of ice sheet, since $A(T)$ does not vary linearly but exponentially. Thus, it can be an order of magnitude larger at the base of the temperature compared to the surface of ice sheet. For our simulations, we calculate $A(T) = 3.5 \times 10^{-25}$ Pa^{-3}s^{-1}, which is the

20 same as A($-10°$C) from Cuffey and Paterson (2010). Incidentally, $-10°C$ is basal temperature of ice sheets at the beginning of inception Marshall et al. (2002), meaning our procedure is capturing the approximate temperature at the base of the ice sheet, which is where flow is more likely with warmer temperatures. Thus, we feel confident in our choice of A for this simulation.

A1   Finite Difference Approximation

We can use the flux form for the finite difference approximation. We use forward Euler and second order centered difference

25 as seen in Figure A3, where n is the time step, i is the node in the x direction, and j is the node in the y direction.

$$\frac{H_{i,j}^{n+1} - H_{i,j}^n}{\Delta t} = \frac{D_{i+\frac{1}{2},j}^n \left(\frac{H_{i+1,j}^{*n} - H_{i,j}^{*n}}{\Delta x_i}\right) + D_{i-\frac{1}{2},j}^n \left(\frac{H_{i,j}^{*n} - H_{i-1,j}^{*n}}{\Delta x_{i-1}}\right)}{\frac{1}{2}(\Delta x_i + \Delta x_{i-1})} + \frac{D_{i,j+\frac{1}{2}}^n \left(\frac{H_{i,j+1}^{*n} - H_{i,j}^{*n}}{\Delta y_j}\right) + D_{i,j-\frac{1}{2}}^n \left(\frac{H_{i,j}^{*n} - H_{i,j-1}^{*n}}{\Delta y_{j-1}}\right)}{\frac{1}{2}(\Delta y_j + \Delta y_{j-1})} + G \tag{A3}$$

The numerical expression for the diffusivity is presented in Equation A7

$$D^n_{i+\frac{1}{2},j} = AH^{m+2}_{i+\frac{1}{2},j}\Big[\Big(\frac{H^*_{i+1,j} - H^*_{i,j}}{\Delta x_i}\Big)^2 + \Big(\frac{1}{2}\Big(\frac{H^*_{i+1,j+1} - H^*_{i+1,j-1}}{\Delta y_{j-1} + \Delta y_j} + \frac{H^*_{i,j+1} - H^*_{i,j-1}}{\Delta y_{j-1} + \Delta y_j}\Big)\Big)^2\Big]^{(m-1)/2} \tag{A4}$$

$$D^n_{i-\frac{1}{2},j} = AH^{m+2}_{i-\frac{1}{2},j}\Big[\Big(\frac{H^*_{i,j} - H^*_{i-1,j}}{\Delta x_{i-1}}\Big)^2 + \Big(\frac{1}{2}\Big(\frac{H^*_{i,j+1} - H^*_{i,j-1}}{\Delta y_{j-1} + \Delta y_j} + \frac{H^*_{i-1,j+1} - H^*_{i-1,j-1}}{\Delta y_{j-1} + \Delta y_j}\Big)\Big)^2\Big]^{(m-1)/2} \tag{A5}$$

$$D^n_{i,j+\frac{1}{2}} = AH^{m+2}_{i,j+\frac{1}{2}}\Big[\Big(\frac{1}{2}\Big(\frac{H^*_{i+1,j+1} - H^*_{i-1,j+1}}{\Delta x_{i-1} + \Delta x_i} + \frac{H^*_{i+1,j} - H^*_{i-1,j}}{\Delta x_{i-1} + \Delta x_i}\Big)\Big)^2 + \Big(\frac{H^*_{i,j+1} - H^*_{i,j}}{\Delta y_j}\Big)^2\Big]^{(m-1)/2} \tag{A6}$$

$$D^n_{i,j-\frac{1}{2}} = AH^{m+2}_{i,j-\frac{1}{2}}\Big[\Big(\frac{1}{2}\Big(\frac{H^*_{i+1,j+1} - H^*_{i-1,j+1}}{\Delta x_{i-1} + \Delta x_i} + \frac{H^*_{i+1,j} - H^*_{i-1,j}}{\Delta x_{i-1} + \Delta x_i}\Big)\Big)^2 + \Big(\frac{H^*_{i,j} - H^*_{i,j-1}}{\Delta y_{j-1}}\Big)^2\Big]^{(m-1)/2} \tag{A7}$$

5 Finally, our use of flux form requires Equation A11.

$$H^{m+2}_{i+\frac{1}{2},j} = \Big(\frac{H_{i+1,j} + H_{i,j}}{2}\Big)^{m+2} \tag{A8}$$

$$H^{m+2}_{i-\frac{1}{2},j} = \Big(\frac{H_{i,j} + H_{i-1,j}}{2}\Big)^{m+2} \tag{A9}$$

$$H^{m+2}_{i,j+\frac{1}{2}} = \Big(\frac{H_{i,j+1} + H_{i,j}}{2}\Big)^{m+2} \tag{A10}$$

$$H^{m+2}_{i,j-\frac{1}{2}} = \Big(\frac{H_{i,j} + H_{i,j-1}}{2}\Big)^{m+2} \tag{A11}$$

10 This model uses a time step of one year. At each time step, a new ice thickness is calculated based the equations above. Then with the new ice thickness and basal topography known, a new surface elevation is calculated ($H^* = B + H$).

The edge and center of the ice sheet can cause $D = 0$, which is unrealistic behavior. Thus, we set a minimum D, but as noted by Oerlemans (1981) and confirmed in our simulations, the ice model does not depend strongly on this choice.

We also characterize the mass balance according to elevation, where G is actually $G(H^*)$. Thus, the mass balance is also
15 updated after each time step, since it depends on H^*. For our main set of simulations, we characterized the mass balance using elevation bins.

Competing interests. The authors declare they have no conflict of interest.

**Climate
of the Past**

Discussions

References

Abe-Ouchi, A., Segawa, T., and Saito, F.: Climatic conditions for modelling the Northern Hemisphere ice sheets throughout the ice age cycle, Climate of the Past, 3, 423–438, 2007.

Abe-Ouchi, A., Saito, F., Kawamura, K., Raymo, M. E., Okuno, J., Takahashi, K., and Blatter, H.: Insolation-driven 100,000-year glacial cycles and hysteresis of ice-sheet volume, Nature, 500, 190–193, 2013.

5   Andrews, J. and Mahaffy, M.: Growth rate of the Laurentide Ice Sheet and sea level lowering (with emphasis on the 115,000 BP sea level low), Quaternary Research, 6, 167–183, 1976.

Beghin, P., Charbit, S., Dumas, C., Kageyama, M., Roche, D., and Ritz, C.: Interdependence of the growth of the Northern Hemisphere ice sheets during the last glaciation: the role of atmospheric circulation, Climate of the Past, 10, 345–358, 2014.

Birch, L., Cronin, T., and Tziperman, E.: Glacial Inception on Baffin Island: The Role of Insolation, Meteorology, and Topography, Journal
10   of Climate, 30, 4047–4064, 2017.

Bonelli, S., Charbit, S., Kageyama, M., Woillez, M.-N., Ramstein, G., Dumas, C., and Quiquet, A.: Investigating the evolution of major Northern Hemisphere ice sheets during the last glacial-interglacial cycle, Climate of the Past, 5, 329–345, 2009.

Bromwich, D. H., Toracinta, E. R., and Wang, S.-H.: Meteorological perspective on the initiation of the Laurentide Ice Sheet, Quaternary International, 95, 113–124, 2002.

15   Bromwich, D. H., Toracinta, E. R., Oglesby, R. J., Fastook, J. L., and Hughes, T. J.: LGM summer climate on the southern margin of the Laurentide Ice Sheet: wet or dry?, Journal of Climate, 18, 3317–3338, 2005.

Calov, R., Ganopolski, A., Petoukhov, V., Claussen, M., Brovkin, V., and Kubatzki, C.: Transient simulation of the last glacial inception. Part II: sensitivity and feedback analysis, Climate Dynamics, 24, 563–576, 2005.

Cassano, J. J., Higgins, M. E., and Seefeldt, M. W.: Performance of the Weather Research and Forecasting model for month-long pan-Arctic
20   simulations, Monthly Weather Review, 139, 3469–3488, 2011.

Chen, S.-H. and Lin, Y.-L.: Orographic effects on a conditionally unstable flow over an idealized three-dimensional mesoscale mountain, Meteorology and Atmospheric Physics, 88, 1–21, 2005.

Clark, P., Clague, J., Curry, B. B., Dreimanis, A., Hicock, S., Miller, G., Berger, G., Eyles, N., Lamothe, M., Miller, B., et al.: Initiation and development of the Laurentide and Cordilleran ice sheets following the last interglaciation, Quaternary Science Reviews, 12, 79–114,
25   1993.

Cook, K. H. and Held, I. M.: Stationary waves of the ice age climate, Journal of climate, 1, 807–819, 1988.

Cosgrove, B. A., Lohmann, D., Mitchell, K. E., Houser, P. R., Wood, E. F., Schaake, J. C., Robock, A., Sheffield, J., Duan, Q., Luo, L., et al.: Land surface model spin-up behavior in the North American Land Data Assimilation System (NLDAS), Journal of Geophysical Research: Atmospheres, 108, 2003.

30   Creveling, J. R., Mitrovica, J. X., Clark, P. U., Waelbroeck, C., and Pico, T.: Predicted bounds on peak global mean sea level during marine isotope stages 5a and 5c, Quaternary Science Reviews, 163, 193–208, 2017.

Cuffey, K. M. and Paterson, W. S. B.: The physics of glaciers, Academic Press, 2010.

de Noblet, N. I., Prentice, I. C., Joussaume, S., Texier, D., Botta, A., and Haxeltine, A.: Possible role of atmosphere-biosphere interactions in triggering the Last Glaciation, Geophysical Research Letters, 23, 3191–3194, 1996.

35   Dee, D. P., Uppala, S. M., Simmons, A. J., Berrisford, P., Poli, P., Kobayashi, S., Andrae, U., Balmaseda, M. A., Balsamo, G., Bauer, P., Bechtold, P., Beljaars, A. C. M., van de Berg, L., Bidlot, J., Bormann, N., Delsol, C., Dragani, R., Fuentes, M., Geer, A. J., Haim-

berger, L., Healy, S. B., Hersbach, H., Hólm, E. V., Isaksen, L., Kållberg, P., Köhler, M., Matricardi, M., McNally, A. P., Monge-Sanz, B. M., Morcrette, J.-J., Park, B.-K., Peubey, C., de Rosnay, P., Tavolato, C., Thépaut, J.-N., and Vitart, F.: The ERA-Interim reanalysis: configuration and performance of the data assimilation system, Quarterly Journal of the Royal Meteorological Society, 137, 553–597, https://doi.org/10.1002/qj.828, http://dx.doi.org/10.1002/qj.828, 2011.

Denis, B., Laprise, R., Caya, D., and Côté, J.: Downscaling ability of one-way nested regional climate models: the Big-Brother Experiment, Climate Dynamics, 18, 627–646, 2002.

Deser, C., Phillips, A. S., Alexander, M. A., and Smoliak, B. V.: Projecting North American climate over the next 50 years: Uncertainty due to internal variability, Journal of Climate, 27, 2271–2296, 2014.

Dong, B. and Valdes, P. J.: Sensitivity studies of Northern Hemisphere glaciation using an atmospheric general circulation model, Journal of Climate, 8, 2471–2496, 1995.

Farrell, B. and Abbot, D.: A mechanism for dust-induced destabilization of glacial climates, Climate of the Past, 8, 2061–2067, 2012.

Ganopolski, A. and Calov, R.: The role of orbital forcing, carbon dioxide and regolith in 100 kyr glacial cycles, Climate of the Past, 7, 1415–1425, 2011.

Ganopolski, A., Calov, R., and Claussen, M.: Simulation of the last glacial cycle with a coupled climate ice-sheet model of intermediate complexity, Climate of the Past, 6, 229–244, 2010.

Gardner, A. S. and Sharp, M.: Influence of the Arctic circumpolar vortex on the mass balance of Canadian high Arctic glaciers, Journal of Climate, 20, 4586–4598, 2007.

Ghil, M.: Cryothermodynamics: The chaotic dynamics of paleoclimate, Physica D: Nonlinear Phenomena, 77, 130–159, 1994.

Gildor, H. and Tziperman, E.: Sea ice as the glacial cycles' climate switch: Role of seasonal and orbital forcing, Paleoceanography, 15, 605–615, 2000.

Gildor, H. and Tziperman, E.: A sea ice climate switch mechanism for the 100-kyr glacial cycles, Journal of Geophysical Research: Oceans, 106, 9117–9133, 2001.

Goñi, M. S., Loutre, M., Crucifix, M., Peyron, O., Santos, L., Duprat, J., Malaizé, B., Turon, J.-L., and Peypouquet, J.-P.: Increasing vegetation and climate gradient in Western Europe over the Last Glacial Inception (122–110 ka): data-model comparison, Earth and Planetary Science Letters, 231, 111–130, 2005.

Goodman, J. C. and Pierrehumbert, R. T.: Glacial flow of floating marine ice in "Snowball Earth", Journal of Geophysical Research: Oceans, 108, 2003.

Gregory, J., Browne, O., Payne, A., Ridley, J., and Rutt, I.: Modelling large-scale ice-sheet-climate interactions following glacial inception, Climate of the Past, 8, 1565, 2012.

Grell, G. A. and Dévényi, D.: A generalized approach to parameterizing convection combining ensemble and data assimilation techniques, Geophysical Research Letters, 29, 2002.

Harvey, L. D.: Milankovitch forcing, vegetation feedback, and North Atlantic deep-water formation, Journal of climate, 2, 800–815, 1989.

Herrington, A. R. and Poulsen, C. J.: Terminating the Last Interglacial: The role of ice sheet–climate feedbacks in a GCM asynchronously coupled to an ice sheet model, Journal of Climate, 25, 1871–1882, 2011.

Hines, K. M., Bromwich, D. H., Bai, L.-S., Barlage, M., and Slater, A. G.: Development and testing of Polar WRF. Part III: Arctic land, Journal of Climate, 24, 26–48, 2011.

Hong, S.-Y. and Lim, J.-O. J.: The WRF single-moment 6-class microphysics scheme (WSM6), Asia-Pacific Journal of Atmospheric Sciences, 42, 129–151, 2006.

Iacono, M. J., Delamere, J. S., Mlawer, E. J., Shephard, M. W., Clough, S. A., and Collins, W. D.: Radiative forcing by long-lived greenhouse gases: Calculations with the AER radiative transfer models, Journal of Geophysical Research: Atmospheres, 113, 2008.

Ives, J.: Indications of Recent Extensive Glacierization in North-Central Baffin Island, NWT, Journal of Glaciology, 4, 197–205, 1962.

Ives, J. D., Andrews, J. T., and Barry, R. G.: Growth and decay of the Laurentide Ice Sheet and comparisons with Fenno-Scandinavia, Naturwissenschaften, 62, 118–125, 1975.

5   Jackson, C.: Sensitivity of stationary wave amplitude to regional changes in Laurentide ice sheet topography in single-layer models of the atmosphere, Journal of Geophysical Research: Atmospheres, 105, 24 443–24 454, 2000.

Jackson, C. and Broccoli, A.: Orbital forcing of Arctic climate: mechanisms of climate response and implications for continental glaciation, Climate Dynamics, 21, 539–557, 2003.

Janjic, Z. I.: The step-mountain eta coordinate model: Further developments of the convection, viscous sublayer, and turbulence closure

10   schemes, Monthly Weather Review, 122, 927–945, 1994.

Jochum, M., Jahn, A., Peacock, S., Bailey, D. A., Fasullo, J. T., Kay, J., Levis, S., and Otto-Bliesner, B.: True to Milankovitch: glacial inception in the new Community Climate System Model, Journal of Climate, 25, 2226–2239, 2012.

Kageyama, M. and Valdes, P. J.: Impact of the North American ice-sheet orography on the Last Glacial Maximum eddies and snowfall, Geophysical Research Letters, 27, 1515–1518, 2000.

15   Kageyama, M., Charbit, S., Ritz, C., Khodri, M., and Ramstein, G.: Quantifying ice-sheet feedbacks during the last glacial inception, Geophysical Research Letters, 31, 2004.

Källén, E., Crafoord, C., and Ghil, M.: Free oscillations in a climate model with ice-sheet dynamics, Journal of the Atmospheric Sciences, 36, 2292–2303, 1979.

Kaspar, F., Spangehl, T., and Cubasch, U.: Northern hemisphere winter storm tracks of the Eemian interglacial and the last glacial inception,

20   Climate of the Past, 3, 181–192, 2007.

Khodri, M., Leclainche, Y., Ramstein, G., Braconnot, P., Marti, O., and Cortijo, E.: Simulating the amplification of orbital forcing by ocean feedbacks in the last glaciation, Nature, 410, 570–574, 2001.

Kilpeläinen, T., Vihma, T., and Ólafsson, H.: Modelling of spatial variability and topographic effects over Arctic fjords in Svalbard, Tellus A, 63, 223–237, 2011.

25   Kleman, J., Fastook, J., and Stroeven, A. P.: Geologically and geomorphologically constrained numerical model of Laurentide Ice Sheet inception and build-up, Quaternary International, 95, 87–98, 2002.

Kleman, J., Fastook, J., Ebert, K., Nilsson, J., and Caballero, R.: Pre-LGM Northern Hemisphere ice sheet topography, Climate of the Past, 9, 2365, 2013.

Kubatzki, C., Claussen, M., Calov, R., and Ganopolski, A.: Sensitivity of the last glacial inception to initial and surface conditions, Climate

30   Dynamics, 27, 333–344, 2006.

Kurtz, N. T. and Farrell, S. L.: Large-scale surveys of snow depth on Arctic sea ice from Operation IceBridge, Geophysical Research Letters, 38, 2011.

Lambeck, K. and Chappell, J.: Sea level change through the last glacial cycle, Science, 292, 679–686, 2001.

Lee, W.-H. and North, G.: Small ice cap instability in the presence of fluctuations, Climate dynamics, 11, 242–246, 1995.

35   Li, C., Battisti, D. S., Schrag, D. P., and Tziperman, E.: Abrupt climate shifts in Greenland due to displacements of the sea ice edge, Geophysical Research Letters, 32, 2005.

Liakka, J. and Nilsson, J.: The impact of topographically forced stationary waves on local ice-sheet climate, Journal of Glaciology, 56, 534–544, 2010.

Liakka, J., Nilsson, J., and Löfverström, M.: Interactions between stationary waves and ice sheets: linear versus nonlinear atmospheric response, Climate dynamics, 38, 1249–1262, 2012.

Löfverström, M., Caballero, R., Nilsson, J., and Kleman, J.: Evolution of the large-scale atmospheric circulation in response to changing ice
5   sheets over the last glacial cycle, Climate of the Past, 10, 1453–1471, 2014.

Marshall, S. and Clarke, G.: Ice sheet inception: subgrid hypsometric parameterization of mass balance in an ice sheet model, Climate Dynamics, 15, 533–550, 1999.

Marshall, S. J. and Clark, P. U.: Basal temperature evolution of North American ice sheets and implications for the 100-kyr cycle, Geophysical Research Letters, 29, 2002.

10   Marshall, S. J., Tarasov, L., Clarke, G. K., and Peltier, W. R.: Glaciological reconstruction of the Laurentide Ice Sheet: physical processes and modelling challenges, Canadian Journal of Earth Sciences, 37, 769–793, 2000.

Marshall, S. J., James, T. S., and Clarke, G. K.: North American ice sheet reconstructions at the Last Glacial Maximum, Quaternary Science Reviews, 21, 175–192, 2002.

Meissner, K., Weaver, A., Matthews, H., and Cox, P.: The role of land surface dynamics in glacial inception: a study with the UVic Earth
15   System Model, Climate Dynamics, 21, 515–537, 2003.

Milankovitch, M.: Kanon der Erdebestrahlung und seine Anwendung auf das Eiszeitenproblem, Königlich Serbische Akademie, 1941.

Niu, G.-Y., Yang, Z.-L., Mitchell, K. E., Chen, F., Ek, M. B., Barlage, M., Kumar, A., Manning, K., Niyogi, D., Rosero, E., et al.: The community Noah land surface model with multiparameterization options (Noah-MP): 1. Model description and evaluation with local-scale measurements, Journal of Geophysical Research: Atmospheres, 116, 2011.

20   Oerlemans, J.: Some basic experiments with a vertically-integrated ice sheet model, Tellus, 33, 1–11, 1981.

Oerlemans, J.: On glacial inception and orography, Quaternary International, 95, 5–10, 2002.

Otieno, F. O. and Bromwich, D. H.: Contribution of Atmospheric Circulation to Inception of the Laurentide Ice Sheet at 116 kyr BP*, Journal of Climate, 22, 39–57, 2009.

Otterman, J., Chou, M., and Arking, A.: Effects of nontropical forest cover on climate, Journal of Climate and Applied Meteorology, 23,
25   762–767, 1984.

Petit, J.-R., Jouzel, J., Raynaud, D., Barkov, N. I., Barnola, J.-M., Basile, I., Bender, M., Chappellaz, J., Davis, M., Delaygue, G., et al.: Climate and atmospheric history of the past 420,000 years from the Vostok ice core, Antarctica, Nature, 399, 429–436, 1999.

Rind, D., Peteet, D., and Kukla, G.: Can Milankovitch orbital variations initiate the growth of ice sheets in a general circulation model?, Journal of Geophysical Research: Atmospheres, 94, 12 851–12 871, 1989.

30   Roe, G. and Lindzen, R.: A one-dimensional model for the interaction between continental-scale ice sheets and atmospheric stationary waves, Climate Dynamics, 17, 479–487, 2001a.

Roe, G. H. and Lindzen, R. S.: The mutual interaction between continental-scale ice sheets and atmospheric stationary waves, Journal of Climate, 14, 1450–1465, 2001b.

Skamarock, W., Klemp, J., Dudhia, J., Gill, D., Barker, D., Duda, M., Huang, X., Wang, W., and Powers, J.: A description of the Advanced
35   Research 488 WRF Version 3, Tech. rep., NCAR Technical Note NCAR/TN-475+ STR. doi: 10.5065/D68S4MVH. 489, 2008.

Smith, R.: The influence of the earth's rotation on mountain wave drag, Journal of the atmospheric sciences, 36, 177–180, 1979.

Van den Berg, J., Van de Wal, R., and Oerlemans, J.: Effects of spatial discretization in ice-sheet modelling using the shallow-ice approximation, Journal of glaciology, 52, 89–98, 2006.

Vavrus, S., Philippon-Berthier, G., Kutzbach, J. E., and Ruddiman, W. F.: The role of GCM resolution in simulating glacial inception, The Holocene, 21, 819–830, 2011.

Vettoretti, G. and Peltier, W.: Post-Eemian glacial inception. Part II: Elements of a cryospheric moisture pump, Journal of Climate, 16, 912–927, 2003.

Vettoretti, G. and Peltier, W.: Sensitivity of glacial inception to orbital and greenhouse gas climate forcing, Quaternary Science Reviews, 23, 499–519, 2004.

Waelbroeck, C., Labeyrie, L., Michel, E., Duplessy, J. C., McManus, J., Lambeck, K., Balbon, E., and Labracherie, M.: Sea-level and deep water temperature changes derived from benthic foraminifera isotopic records, Quaternary Science Reviews, 21, 295–305, 2002.

Wang, Z. and Mysak, L. A.: Simulation of the last glacial inception and rapid ice sheet growth in the McGill Paleoclimate Model, Geophysical Research Letters, 29, 2002.

Wang, Z., Cochelin, A.-S. B., Mysak, L. A., and Wang, Y.: Simulation of the last glacial inception with the green McGill Paleoclimate Model, Geophysical research letters, 32, 2005.

Weertman, J.: Deformation of floating ice shelves, Journal of glaciology, 3, 38–42, 1957.

Yang, Z.-L., Dickinson, R., Henderson-Sellers, A., and Pitman, A.: Preliminary study of spin-up processes in land surface models with the first stage data of Project for Intercomparison of Land Surface Parameterization Schemes Phase 1 (a), Journal of Geophysical Research: Atmospheres, 100, 16 553–16 578, 1995.

Yin, J. H. and Battisti, D. S.: The importance of tropical sea surface temperature patterns in simulations of Last Glacial Maximum climate, Journal of Climate, 14, 565–581, 2001.

Yoshimori, M., Reader, M., Weaver, A., and McFarlane, N.: On the causes of glacial inception at 116 kaBP, Climate Dynamics, 18, 383–402, 2002.

Zdanowicz, C., Smetny-Sowa, A., Fisher, D., Schaffer, N., Copland, L., Eley, J., and Dupont, F.: Summer melt rates on Penny Ice Cap, Baffin Island: Past and recent trends and implications for regional climate, Journal of Geophysical Research: Earth Surface, 117, 2012.